Cerrahpaşa Med J 2023; 47(3): 306-312 ORIGINAL ARTICLE

Prediction of Hydrocephalus in Colloid Cysts Using Artificial Intelligence

Basak Atalay, Mahmut Bilal Dogan, Mehmet Bilgin Eser

Department of Radiology, Goztepe Suleyman Yalcin City Hospital, Istanbul Medeniyet University Faculty of Medicine, Istanbul, Turkey

Cite this article as: Atalay B, Dogan MB, Eser MB. Prediction of hydrocephalus in colloid cysts using artificial intelligence. *Cerrahpaşa Med J.* 2023;47(3):306-312.

Abstract

Objective: We aim to train neural networks to predict hydrocephaly in patients with colloid cysts based on T2-weighted magnetic resonance imaging radiomics.

Methods: This study included 40 cases with a colloid cyst; the mean age was 54.08 ± 16.57 years, and 25 (62.5%) were women. Two observers segmented cysts on axial T2-weighted MRI and evaluated conventional features. Predictors were radiomics (n = 851) and conventional features (n = 12). Feature selection was based on coefficient variance (CoV), variance inflation factor (VIF), and least absolute shrinkage, and a selection operator regression analysis. The outcome was identified as hydrocephaly. Models were developed with artificial neural networks (ANN) for 3 different diagnostic prediction models. The first model included radiomics features; the second model included conventional features; and the third model included all of the features. Artificial neural network performance was presented as an area under curve (AUC) and the receiver operating characteristic curve (ROC) and accepted as successful if the AUC > 0.85 and *p*-value < .01.

Results: By using CoV and VIF analysis, 49 features were found to be stable. Radiomics predict hydrocephaly with AUC = 0.88, sensitivity: 92%, specificity: 97%. Conventional features predict hydrocephaly with AUC = 0.87, sensitivity: 82%, and specificity: 93%. Third model (radiomics+ conventional) AUC was 0.99, sensitivity: 91%, and specificity: 100% (all *p*-values < .001).

Conclusion: This study was successful in training neural networks that can predict hydrocephaly in patients with colloid cysts.

Keywords: Colloid cysts, magnetic resonance imaging, computer-assisted image processing, machine learning, artificial intelligence

Introduction

The colloid cyst of the third ventricle can cause acute and profound hydrocephalus. In some cases, colloid cysts are associated with sudden death. They compose 0.5% to 1% of brain tumors. It is usually silent in childhood and may become symptomatic in the third and fourth decades of life. The cyst content (mucin, hemorrhage, and cholesterol) and degree of hydration determine the imaging characteristic. The colloid cysts are generally well-circumscribed, round–oval, and hyperdense on computed tomography (CT).[1-4] The signal intensity of the cyst in magnetic resonance imaging (MRI) depends on the content. Thin rim enhancement may be seen in the cyst wall, and no calcification is seen.[1,5] The colloid cyst can be easily distinguished from other cystic lesions such as epidermoid, dermoid, and ependymal cysts with its location and typical imaging features. A scoring system was proposed to predict hydrocephalus in asymptomatic patients, and it was suggested that the treatment had a positive effect on the neural cognition of patients.[4,6,7]

Radiomics is a method that obtains quantitative data from radiological images that have been used in the last decade. In oncology, it is widely used to predict tumor histology, chemoradiotherapy response, and even patient survival.[8-11] Due to the multidimensional nature of radiomics data, the use of artificial intelligence in feature selection and model development is increasing.[12] In this study, neural networks were based on multilayer perceptron (MLP) and radial basis function (RBF). All configured networks are feed-forward and fully connected.

This study aimed to train neural networks to predict hydrocephaly in patients with colloid cysts based on T2-weighted (T2W) MRI radiomics.

Methods

Ethical Considerations

A retrospective model-development study was done after the university's local ethics committee approval (Decision number: 2021/0306). Since it is a retrospective study, written informed consent was waived. This study was performed in accordance with the ethical standards laid down in the 1964 Declaration of Helsinki and its later amendments and the Standards for Reporting Diagnostic Accuracy statement was followed.[13]

Study Population and Data Collection

We conducted a keyword search of "colloid cyst" in radiology reports to identify patients with colloid cysts. Patients who had only CT images or MRIs without a T2W sequence were excluded from the study. Among the patients, 40 consecutive cases with colloid cysts between January 2015 and January 2020 were included. Age, gender, and clinical findings (presence or absence of headache) were determined from the hospital data system. The dimensions of the colloid cyst, FLAIR hyperintensity of the colloid cyst, risk zone location, and signal intensity changes in periventricular white matter were noted from MR images. The colloid cyst

Received: December 08, 2022 **Accepted:** May 31, 2023
Publication Date: November 30, 2023
Corresponding author: Basak Atalay, Department of Radiology, Istanbul Medeniyet University Faculty of Medicine, Istanbul, Turkey
e-mail: basak_hosgoren@yahoo.com
DOI: 10.5152/cjm.2023.22118

risk scores (CCRS) were calculated and added to the worksheet.[4] Patients with an Evans index above 0.30 were accepted as having hydrocephalus.

Predictors and Outcomes

Magnetic resonance image of the included patients was taken from the hospital archive and anonymized. Resampling and normalization were made. Segmentation was done volumetrically on T2-weighted MRI images using 3D Slicer software (Figure 1), version 4.10.2 (https://www.slicer.org), blinded to patient outcome data. Eight hundred fifty-one radiomic features were extracted with PyRadiomics, version 2.2.0. All the features (shape, first order, and high order) in this module were selected, and wavelet-based filters were activated. Other detailed information about the radiomic features included in the study is provided in Table 1. Predictors were identified as radiomic features (n = 851) and conventional features (n = 12). The CCRS and the other determined conventional features are presented in Table 2. The outcome was defined as the presence of hydrocephalus (11/40, Figure 2).

Multidimensionality Reduction and Feature Selection

Stability of an image biomarker means that it is minimally affected by the sources of the differences in image acquisition, method, and human interface (low coefficient of variance or standard deviation), has a low relativity error rate (address accuracy), and suitable for clinical translation (diagnostic, therapeutic, and prognostic value) as determined by the European Society of Radiology (ESR).[14-16]

Feature selection was based on coefficient variance (CoV), variance inflation factor (VIF), and least absolute shrinkage, and a selection operator (LASSO) regression analysis. [14,17,18] Features were taken into the CoV analysis and those with >15% variance were eliminated. Features that passed the CoV analysis were further subjected to Spearman's correlation analysis, and correlation matrixes were performed for VIF analysis. Variance inflation factor analyses were performed to reduce the colli nearity–multicollinearity using the formula $1/1 - R^2$. If the VIF was above 10, the feature was eliminated. Finally, features were selected with the LASSO with random sampling, and 5-fold cross-validation was used.

Structuring Automated Neural Networks

Neural networks were trained to develop a diagnostic model. For training, networks of MLP and RBF were selected. The software randomly sampled 40% of the cases as train (n = 12 control vs. n = 4 event), 20% as test (n = 5 control vs. n = 3 event), and 40% as validation (n = 12 control vs. n = 4 event) set. The software assigned the number of neurons (6-25), number of bias neurons (minimum 1 per hidden layer), and number of layers [input layer (n = predictors for RBF and n = predictors + bias neuron for MLP), minimum 2 hidden layers, output layer (n = 2, positive event or not)], activation-hidden-output function [identity, logistic sigmoid, hyperbolic tangent, exponential, Softmax, and Gaussian (only available for RBF networks)], and error function (sum of squares, cross entropy), in these models by evaluating data (Table 3). With these settings, we trained 1000 networks and retained the most successful ones for each condition. The first model included the selected radiomic features, the second model included conventional features, and the third model included the selected radiomic features and conventional features as the predictors.

Statistical analyses, neural network training, and validation were performed using TIBCO Statistica version 13.0.5 (Palo Alto, Calif, USA). Neural network results are presented with area under the curve (AUC) and 95% confidence intervals. In receiver operating curve (ROC) analysis, if AUC > 0.85 and $p < .01$, then it is considered a validated classifier neural network.

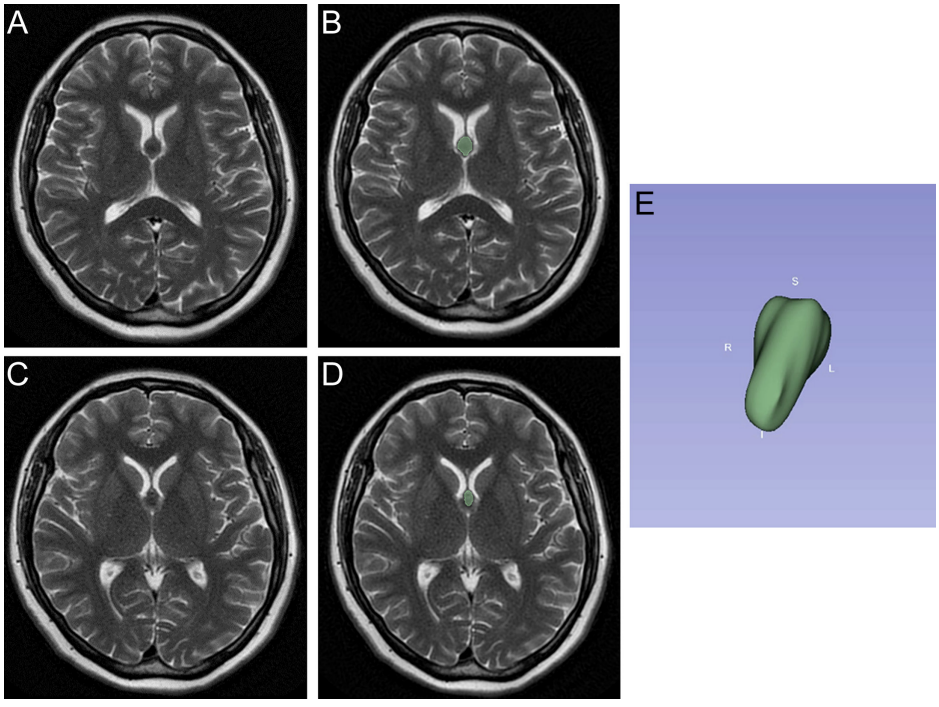

Figure 1. Magnetic resonance imaging in a 46-year-old female presenting with headache. (A and C) Axial T2-weighted spin-echo images show a rounded, hypointense mass in the anterior aspect of the third ventricle. (B and D) The segmentation of colloid cysts at the same level is shown. (E) 3D volume rendering AP projection obtained by segmentation from T2-weighted sequences shows the colloid cyst. (AP, anteroposterior)

Table 1. Extracted Radiomic Features as per Categories and Subcategories

		High Order Textural Features				
Shape and Size Features (n = 14 × 1)	**First Order Features (n = 18 × 9)**	**GLDM (n = 14 × 9)**	**GLCM (n = 24 × 9)**	**GLRLM (n = 16 × 9)**	**GLSZM (n = 16 × 9)**	**NGTDM (n = 5 × 9)**
1. Voxel volume 2. Maximum 3D diameter 3. Mesh volume 4. Major axis length 5. Sphericity 6. Least axis length 7. Elongation 8. Surface volume ratio 9. Maximum 2D diameter 10. Slice flatness 11. Surface area 12. Minor axis length 13. Maximum 2D diameter column 14. Maximum 2D diameter row	1. Interquartile range 2. Skewness 3. Uniformity 4. Median 5. Energy 6. Robust mean absolute deviation 7. Mean absolute deviation 8. Total energy 9. Maximum 10. Root mean squared 11. 90 percentile 12. Minimum 13. Entropy 14. Range 15. Variance 16. 10 percentile 17. Kurtosis 18. Mean	1. Gray level variance 2. High gray level emphasis 3. Dependence entropy 4. Dependence non-uniformity 5. Gray level non-uniformity 6. Small dependence emphasis 7. Small dependence high gray level emphasis 8. Dependence non-uniformity normalized 9. Large dependence emphasis 10. Large dependence low gray level emphasis 11. Dependence variance 12. Large dependence high gray level emphasis 13. Small dependence low gray level emphasis 14. Low gray level emphasis	1. Joint average 2. Sum average 3. Joint entropy 4. Cluster shade 5. Max probability 6. Inverse DM normalized 7. Joint energy 8. Contrast 9. Difference entropy 10. Inverse variance 11. Difference variance 12. ID normalized 13. ID moment 14. Correlation 15. Autocorrelation 16. Sum entropy 17. MCC 18. Sum squares 19. Cluster prominence 20. IMC2 21. IMC1 22. Difference average 23. ID 24. Cluster tendency	1. Short run low gray level emphasis 2. Gray level variance 3. Low gray level run emphasis 4. GL non-uniformity normalized 5. Run variance 6. Gray level non-uniformity 7. Long run emphasis 8. Short run high gray level emphasis 9. Run length non-uniformity 10. Short run emphasis 11. Long run high gray level emphasis 12. Run percentage 13. Long run low gray level emphasis 14. Run entropy 15. High gray level run emphasis 16. Run length non-uniformity normalized	1. Gray level variance 2. Zone variance 3. Gray level non-uniformity normalized 4. Size zone non-uniformity normalized 5. Size zone non-uniformity 6. Gray level non-uniformity 7. Large area emphasis 8. Small area high gray level emphasis 9. Zone percentage 10. Large area low gray level emphasis 11. Large area high gray level emphasis 12. High gray level zone emphasis 13. Small area emphasis 14. Low gray level zone emphasis 15. Zone entropy 16. Small area low gray level emphasis	1. Coarseness 2. Complexity 3. Strength 4. Contrast 5. Busyness

One hundred seven features were extracted from the original image, and shape and size features were extracted only for the original image. This study was used 8 different wavelet filters, and 93 features from each were extracted. Thus, a total of 851 features were extracted for each image. The 8 filters are described in detail in the PyRadiomics document (https://pyradiomics.readthedocs.io/en/latest/customization.html#enabled-features).2D, two-dimensional; 3D, three-dimensional; GLCM, gray-level co-occurrence matrix; GLDM, gray-level dependence matrix; GLRLM, gray-level run length matrix; GLSZM, gray-level size zone matrix; ID, inverse difference; IMC, informational measure of correlation; MCC, maximal correlation coefficient; NGTDM, neighboring gray-tone difference matrix; GL, gray level.

Table 2. Conventional Features, Descriptions, and Distributions

Feature	Type	Description	Distributions with n
Gender	Categorical	1. Female, 2. Male	25 female, 15 male
Age	Quantitative	Years (mean ± SD)	54.08 ± 16.57
Cyst dimensions	Quantitative	AP × TR × CC with millimeters (mean ± SD)	7.88 ± 3.81 × 7.25 ± 3.38 × 7.20 ± 3.84 mm
Periventricular hyperintensity	Categorical	0. No, 1. Yes	36 no, 4 yes
Colloid cyst risk score	Categorical	It consists of 5 conventional features	S0: 0, S1: 5, S2: 5, S3: 15, S4: 7, S5: 7
Age <65 years	Categorical	0. No, 1. Yes	13 no, 27 yes
Headache	Categorical	0. No, 1. Yes	15 no, 25 yes
Axial cyst diameter >7 mm	Categorical	0. No, 1. Yes	16 no, 24 yes
FLAIR hyperintensity	Categorical	0. No, 1. Yes	21 no, 19 yes
Risk zone	Categorical	0. No, 1. Yes	4 no, 36 yes

The quantitative features used in the study were age and the 3 dimensions of the colloid cyst. Also, age and axial cyst diameter were included as categorical features as part of the colloid cyst risk score (CCRS). Risk zone is lesions located in the zones I and III, shown in Figure 3. All of these 10 features have been used as a predictor feature in model 2. The third model were used as predictor of first and second model's predictors. FLAIR, Fluid attenuated inversion recovery; AP, antero-posterior; TR, Transvers; CC, craniocaudal.

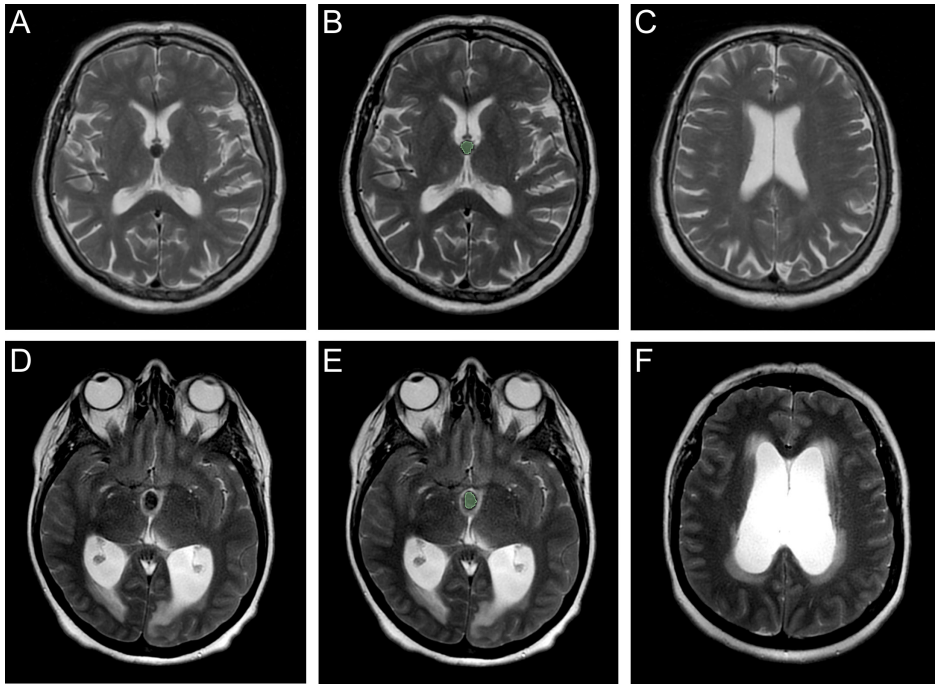

Figure 2. (A and B) Colloid cyst and segmentation are seen on T2-weighted magnetic resonance images in a 49-year-old female patient. C It is observed that ventricle dimensions are normal in the same patient. (B and E) A 71-year-old female patient has a colloid cyst and its segmentation on T2-weighted magnetic resonance images. (F) Hydrocephalus is seen in the same patient.

Table 3. Model Structure and Configurations

	Number of Inputs	Structure	Training Algorithm	Error Function	Hidden Activation	Output Activation
Model 1	5	RBF	RBFT	SOS	Gaussian	Identity
Model 2	10	MLP	BFGS	SOS	Exponential	Exponential
Model 3	15	RBF	RBFT	Entropy	Gaussian	Identity

MLP, multilayer perceptron; RBF, radial basis function; RBFT, Redundant Byzantine Fault Tolerance; BFGS, Broyden-Fletcher-Goldfarb-Shanno; SOS, Sum of Squares.

Table 4. Results for Trained Networks

	True Positive	False Positive	True Negative	False Negative	Area Under Curve	Accuracy %
Model 1	9	2	27	2	0.87	90.00
Model 2	9	2	28	1	0.88	92.50
Model 3	10	0	29	1	0.99	97.50

Results

Patient's Characteristics

This study included 40 cases; the mean age was 54.08 ± 16.57 years, and 25/40 (62.5%) were women. The clinical and radiologic characteristics are presented in Table 2.

Feature Selection

In total, 851 features were evaluated by CoV, and 779 features were eliminated. Another 23 features were eliminated by VIF analysis due to collinearity. Most of the radiomic features were found to be unstable (n = 802, 94%).

Diagnostic Prediction Model Results

Radiomic features predict hydrocephaly with AUC = 0.88, p < .001, sensitivity: 92%, and specificity: 97%. Conventional features predict hydrocephaly with AUC = 0.87, *P* < .001, sensitivity: 82%, and specificity: 93%. Combination of conventional and radiomic features (Third model) AUC was 0.99, *P* < .001, sensitivity: 91%, specificity: 100% (Table 4 and Figure 3).

Discussion

All 3 neural networks achieved targeted diagnostic accuracy in predicting hydrocephaly in patients with colloid cysts. However, the most successful model was the third, created by combining

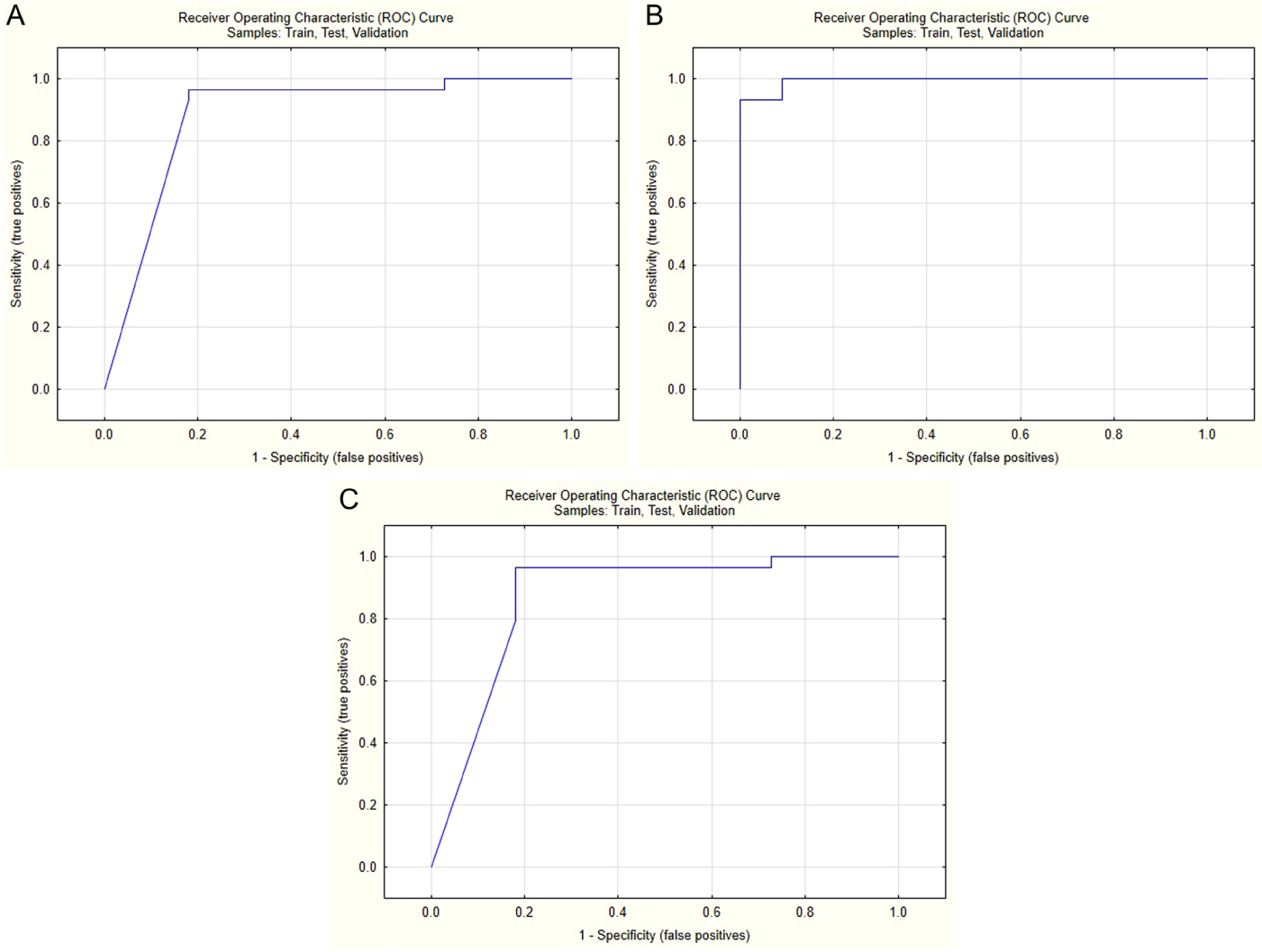

Figure 3. Receiver operating characteristic curves for conventional features, radiomic features, and combination of conventional and radiomic features, respectively.

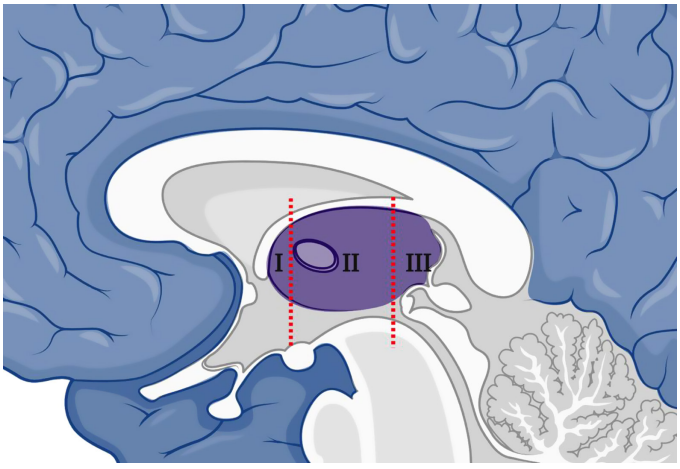

Figure 4. The third ventricle was divided into 3 zones along the sagittal axis to determine the risk zone: zone I, from the lamina terminalis to the massa intermedia; zone II, from the massa intermedia to the inlet of the cerebral aqueduct; and zone III, from the inlet of the cerebral aqueduct to the posterior of the third ventricle.

conventional and radiomic features. With the new pipeline used in this study, we have shown that many radiomic features were not stable.

Previous studies in neuroradiology focused on oncology, especially glioblastoma diagnosis, surveillance, and chemotherapy response.[10-12] Radiomic features that make these distinctions take advantage of the heterogeneity of the tumor.[9] The search for the keywords glioblastoma and radiomics in the PubMed search yields approximately 276 results (July 2022). In this study, we focused on the nononcologic use of radiomics. The CCRS is a scoring system that predicts the development of hydrocephalus, and it is unclear which of the parameters used in scoring is more effective in the development of hydrocephalus. Acute obstructive hydrocephalus and serious complications such as herniation, infarction, and death may occur in patients with colloid cysts.[19] Therefore, the prediction of hydrocephalus is critical. Depending on the protein density, colloid cysts may appear hyperdense on CT, hypointense in the T2W sequence, and hyperintense in the T1W sequence.[20] We hypothesized that differences in intensity and heterogeneity in colloid cysts that the naked eye cannot distinguish might predict hydrocephalus. According to the current study results, neural networks, configured with radiomic data, successfully predicted whether patients had hydrocephalus.

In a recent study, colloid cysts were scored over 5 points, with scoring based on age, history of headaches, axial size of the cyst, FLAIR hyperintensity, and lesion localization (Figure 4). Patients who got 4 and 5 points from this scoring developed hydrocephalus in their follow-up and became symptomatic. The AUC for symptomatic colloid cysts and obstructive hydrocephalus was 0.98 and 0.94, respectively.[6] Our study's second model similarly reached 0.87 AUC using only conventional features. However, the third model, which used all features, had the highest success, and this model accurately predicted hydrocephalus in 40 participants, except for 1 patient. To the best of our knowledge, this is the first study to use T2-weighted MRI radiomics in the diagnosis of hydrocephalus in patients with colloid cysts.

Another important addition to the pipeline is that the data are evaluated with fully automated neural networks. What we mean by automatization here is that the involvement of the human observer is minimized. Unlike previous studies, software independently decided how many neurons to be in the model, which configuration, how many layers to be, which training algorithm to choose, which error function to use, which hidden activation to use, and which output activation to use for evaluating predictors and outcomes (Figure 5).

Limitations

Our study has several limitations. The first of these is that the study is single centered, and the sample size is limited. The second limitation is the disproportionate distribution between the patients with hydrocephalus and patients without hydrocephalus. We used all available internal validation options to deal with this limitation.

This study could not train a convolutional neural network for this task due to the sample size limitation.[21] The community's need for large case-imaging libraries that can accommodate all kinds of cases in every field of medicine is increasing.

Conclusion

This study successfully trained and validated neural networks that can predict hydrocephaly in patients with colloid cysts.

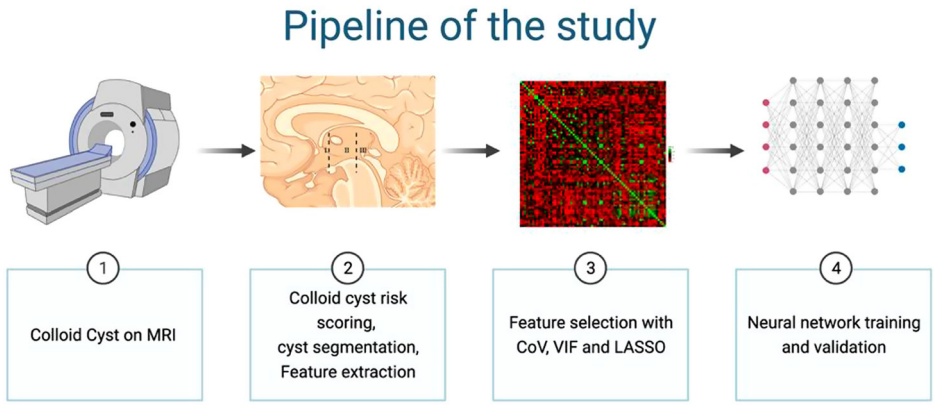

Figure 5. The pipeline of the study. Coefficient of variance and variance inflation factor analyses added to the pipeline significantly reduced multidimensionality. These analyses also allowed the selection of the most stable and diverse features. The automated neural networks used have reduced human-induced bias to a minimum.

Ethics Committee Approval: Ethical committee approval was received from the Ethics Committee of Istanbul Medeniyet University (Approval no: 2021/0306, Date: 16.06.2021).

Informed Consent: Written informed consent was obtained from the patients who agreed to take part in the study.

Peer-review: Externally peer-reviewed.

Author Contributions: Concept – B.A., M.B.E.; Design – B.A., M.B.E., M.B.D.; Supervision – B.A.; Resources – B.A., M.B.E., M.B.D.; Materials – B.A., M.B.E., M.B.D.; Data Collection and/or Processing – M.B.E., M.B.D.; Analysis and/or Interpretation – B.A., M.B.E.; Literature Search – B.A., M.B.E., M.B.D.; Writing Manuscript – B.A., M.B.E., M.B.D.; Critical Review – B.A., M.B.E., M.B.D.

Acknowledgments: Figure 4 was created with BioRender.com. This study was presented in the European Congress of Radiology, March 3-7, 2021, Vienna, Austria.

Declaration of Interests: The authors have no conflict of interest to declare.

Funding: The authors declared that this study has received no financial support.

References

1. Vandesteen L, Drier A, Galanaud D, et al. Imaging findings of intraventricular and ependymal lesions. *J Neuroradiol*. 2013;40(4):229-244. [CrossRef]
2. Musa G, Simfukwe K, Gots A, Chmutin G, Chmutin E, Chaurasia B. Clinical and radiological characteristics in fatal third ventricle colloid cyst. Literature review. *J Clin Neurosci*. 2020;82(A):52-55. [CrossRef]
3. Cuoco JA, Rogers CM, Busch CM, Benko MJ, Apfel LS, Elias Z. Postexercise death due to hemorrhagic colloid cyst of third ventricle: case report and literature review. *World Neurosurg*. 2019;123:351-356. [CrossRef]
4. Beaumont TL, Limbrick DD Jr, Rich KM, Wippold FJ 2nd, Dacey RG Jr. Natural history of colloid cysts of the third ventricle. *J Neurosurg*. 2016;125(6):1420-1430. [CrossRef]
5. Yildiz AE, Oguz KK, Fitoz S. Suprasellar masses in children: characteristic MR imaging features. *J Neuroradiol*. 2016;43(4):246-259. [CrossRef]
6. Zeineddine HA, Westmark K, Khanpara S, et al. Risk analysis and management of third ventricular colloid cysts. *World Neurosurg*. 2021;146:e1071-e1078. [CrossRef]
7. Roth J, Sela G, Andelman F, Nossek E, Elran H, Ram Z. The impact of colloid cyst treatment on neurocognition. *World Neurosurg*. 2019;125:e372-e377. [CrossRef]
8. Park JE, Kim D, Kim HS, et al. Quality of science and reporting of radiomics in oncologic studies: room for improvement according to radiomics quality score and TRIPOD statement. *Eur Radiol*. 2020;30(1):523-536. [CrossRef]
9. Gillies RJ, Kinahan PE, Hricak HH. Images are more than pictures, they are data. *Radiology*. 2016;278(2):563-577. [CrossRef]
10. Bhandari AP, Liong R, Koppen J, Murthy SV, Lasocki A. Noninvasive determination of IDH and 1p19q status of lower-grade gliomas using MRI radiomics: a systematic review. *AJNR Am J Neuroradiol*. 2021;42(1):94-101. [CrossRef]
11. Wagner MW, Hainc N, Khalvati F, et al. Radiomics of pediatric low-grade gliomas: toward a pretherapeutic differentiation of BRAF-mutated and BRAF-fused tumors. *AJNR Am J Neuroradiol*. 2021;42(4):759-765. [CrossRef]
12. Lao J, Chen Y, Li ZC, et al. A deep learning-based radiomics model for prediction of survival in glioblastoma multiforme. *Sci Rep*. 2017;7(1):10353. [CrossRef]
13. Bossuyt PM, Reitsma JB, Bruns DE, et al. STARD 2015: an updated list of essential items for reporting diagnostic accuracy studies. *Radiology*. 2015;277(3):826-832. [CrossRef]
14. European Society of Radiology (ESR). ESR statement on the validation of imaging biomarkers. *Insights Imaging*. 2020;11(1):76. [CrossRef]
15. Traverso A, Kazmierski M, Shi Z, et al. Stability of radiomic features of apparent diffusion coefficient (ADC) maps for locally advanced rectal cancer in response to image pre-processing. *Phys Med*. 2019;61:44-51. [CrossRef]
16. Traverso A, Kazmierski M, Welch ML, et al. Sensitivity of radiomic features to inter-observer variability and image pre-processing in apparent diffusion coefficient (ADC) maps of cervix cancer patients. *Radiother Oncol*. 2020;143:88-94. [CrossRef]
17. Kim JH. Multicollinearity and misleading statistical results. *Korean J Anesthesiol*. 2019;72(6):558-569. [CrossRef]
18. Tibshirani R. Regression shrinkage and selection via the lasso. *J R Stat Soc B*. 1996;58(1):267-288. [CrossRef]
19. Ozmen E, Algin O. Blindness: an uncommon presentation of colloid cysts. *Sultan Qaboos Univ Med J*. 2014;14(1):e128-e129. [CrossRef]
20. Algin O, Ozmen E, Arslan H. Radiologic manifestations of colloid cysts: a pictorial essay. *Can Assoc Radiol J*. 2013;64(1):56-60. [CrossRef]
21. Balki I, Amirabadi A, Levman J, et al. Sample-size determination methodologies for machine learning in medical imaging research: a systematic review. *Can Assoc Radiol J*. 2019;70(4):344-353. [CrossRef]